

REVIEW

Open Access

Carbon doping induced imperfections on MgB₂ superconducting wire

Jung Ho Kim¹ and Seyong Choi^{2*}

Abstract

Carbon is known to be the most effective dopant for magnesium diboride, MgB₂, especially for enhancing high-field electrical properties. Carbon increases the impurity scattering rate, and this, combined with the two-band nature of MgB₂, raises the upper critical field and thereby the high-field critical current. In addition, microscopic analysis has shown that carbon doping induces crystalline imperfections as the origin of impurity scattering. Herein, further detailed transmission electron microscopy analysis has been applied to find more clues for understanding the role of carbon.

Keywords: Carbon doping; Impurity scattering; MgB₂ superconducting wire; Microscopic origin

Review

Magnesium diboride, MgB₂, has been regarded as a very promising candidate for alternatively commercial superconducting materials (Nagamatsu et al. 2001). Together with its simple crystalline structure and low material cost, the transition temperature around 40 K enabling a cryogen-free operation is definitely attractive for engineering applications (Patel et al. 2014). Even if MgB₂ has many advantages, it still has drawbacks in terms of material synthesis. For example, two key precursors such as magnesium and boron are very sensitive to air, especially oxygen, resulting in MgO and B₂O₃ as impurity phases (Kim et al. 2007). In addition, a large difference in the melting temperature between the two precursors makes MgB₂ a complicated reaction (Hata et al. 2013).

For making a wire/tape conductor, a normal *in situ* process has been applied with a specific dopant, i.e., carbon. The introduction of carbon dopant for impurity scattering is to increase the upper critical field and thereby enhance the high-field critical current density. When carbon substitutes boron sites of the MgB₂ structure, shrinkage of the *a*-axis parameter occurs (Kazakov et al. 2005; Kortus et al. 2005). There can be a decrease in the density of state (DOS) and hardening of the optical *E*_{2g} phonons which is known to be strongly related

with the superconducting properties of MgB₂ (Eisterer 2007). According to our previous report (Kim et al. 2012), however, the studies employing microscopic tools such as scanning transmission electron microscopy (STEM) and electron energy loss spectroscopy (EELS) did not show direct evidence on how boron sites are replaced by carbon. The main reason is the limitation (<1 at.% carbon) of the EELS resolution. A recent work on the STEM observation of a MgB₂ specimen sintered at a low temperature (650°C) and short sintering time (<1 h) still remains unclear because the majority of carbon was found to be mainly located at the grain boundaries (Susner et al. 2014). In this work, as an extension of our previous work, detailed structural analysis and microstructure observations have been further carried out with an electrical current carrying property of a MgB₂ superconductor.

The chemical solution process via a carbohydrate has become popular and advantageous in terms of both cost and performance (Kim et al. 2012). For this study, MgB₂ was fabricated by the *in situ* powder-in-tube process (Jin et al. 2011). After dissolving 10 wt.% malic acid (C₄H₆O₅, 99.0%) in toluene (C₇H₈, 99.5%), the solution was mixed with an appropriate amount of boron (B, 99.9%) powder in a Spex mill (Spex Industries Inc., Metuchen, NJ, USA) for 10 min (100 rpm). The slurry was dried at 150°C in a dry oven to form a coating around boron powder particles (that is, carbon encapsulated boron). This uniform composite was then mixed with magnesium (Mg, 99%) powder and mixed in a Fritsch planetary mill (Fritsch, Idar-Oberstein, Germany; 500 rpm) for 10 min. The mixed

* Correspondence: sychoi07@kbsi.re.kr

²Busan Center, Korea Basic Science Institute, Geumjeong, Busan 609-735, Republic of Korea

Full list of author information is available at the end of the article

powder was packed into a 140-mm-long iron (Fe) tube. The outer and inner diameters of the Fe tube were 10 and 8 mm, respectively. The packed tube was drawn till the final outer diameter became 0.83 mm. The fabricated wires were sintered at 650°C for 30 min under high-purity argon gas with a ramp rate of 5°C min⁻¹.

For microstructures, we used a JEOL Cs-corrected dedicated scanning transmission electron microscope (STEM; JEM-2500SES, JEOL Ltd. Tokyo Japan) equipped with a Gatan 766 EELS spectrometer (Enfina 1000, Gatan, Inc., Pleasanton, CA, USA). The specimens for transmission electron microscopy (TEM) observation were prepared by a wedge polishing method and then ion-milled with a low accelerating voltage (0.1 keV). High-angle annular dark-field (HAADF) images were obtained with a beam size of about 1 Å at the condition of the HAADF detector inner cutoff angle in 113 mrad. In addition, high-resolution TEM observation was conducted in a JEOL 300-keV field emission transmission electron microscope (FE-TEM, JEM-3000F).

The field and temperature dependences of the critical current density for the malic acid-doped sample are shown in Figure 1a. Transport current up to 400 A was measured by the standard four-probe method with a criterion of 1 μV cm⁻¹. The temperature dependence was also studied by a variable temperature insert (VTI) system. The critical current density of the malic acid-doped wire was estimated to be 105 A cm⁻² at 6 T and 4.2 K, which is comparable to the critical current density of commercial Nb-Ti wires under the same condition (Kim et al. 2012). Even at higher temperature (20 K), the critical current density in the malic acid-doped MgB₂ wire also exceeds 104 A cm⁻² at 5 T. These critical current density values are the highest record published so far for an *in situ* processed wire. The measured critical temperature for the doped wire was estimated to be 34 K. It should be noted that the critical currents of the doped sample can be described by the percolation model (Kim et al. 2011; Maeda et al. 2013). All the fitting lines in Figure 1a were calculated from the percolation theory and are in good agreement with the measured data. The field dependence of the critical current density can be numerically fitted by the following integral equation:

$$J_c = \int_0^{\infty} \left(\frac{p(J) - P_c}{1 - P_c} \right)^{1.79} dJ \quad (1)$$

where $p(J)$ is the fraction of grains with a critical current density above J and P_c is the percolation threshold, the minimum fraction required for a superconducting current flow. The critical current of each grain is calculated with a grain boundary pinning model: $J_c = F_m \cdot (1 - B/B_{c2})^2 / \sqrt{B_{c2} B}$, where F_m is the pinning force maximum. The upper critical field, B_{c2} , has an angular dependence, which

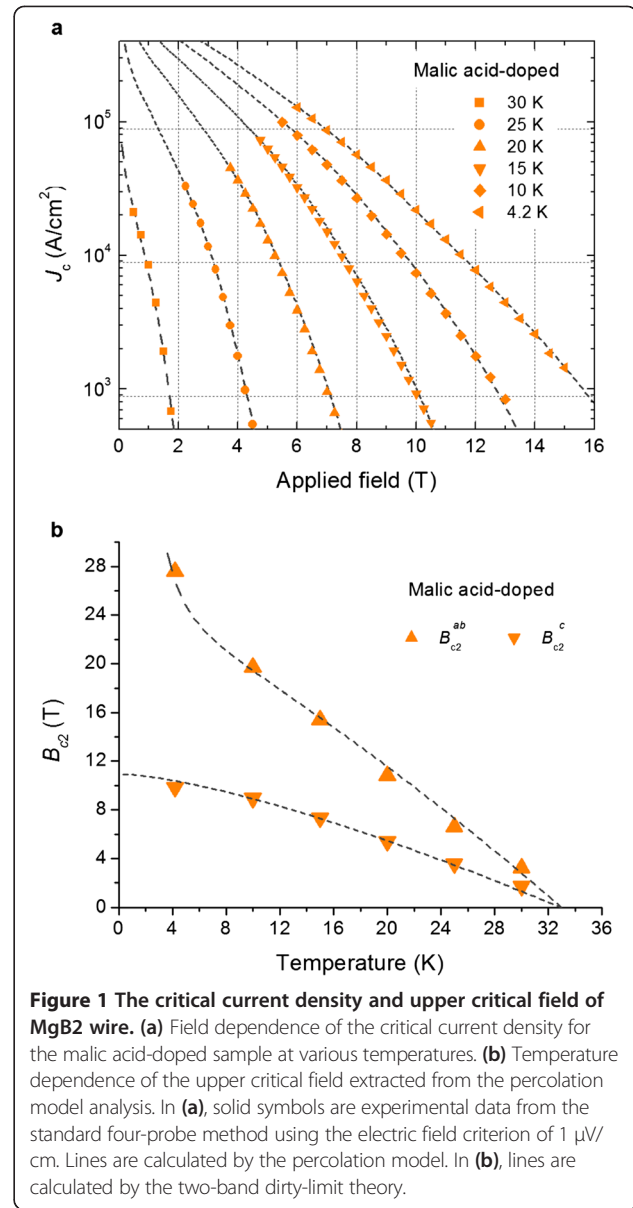


Figure 1 The critical current density and upper critical field of MgB₂ wire. **(a)** Field dependence of the critical current density for the malic acid-doped sample at various temperatures. **(b)** Temperature dependence of the upper critical field extracted from the percolation model analysis. In **(a)**, solid symbols are experimental data from the standard four-probe method using the electric field criterion of 1 μV/cm. Lines are calculated by the percolation model. In **(b)**, lines are calculated by the two-band dirty-limit theory.

can be described by $B_{c2}(\theta) = B_{c2}^{ab} / \sqrt{\gamma^2 \cos^2(\theta) + \sin^2(\theta)}$, from the anisotropic Ginzburg-Landau theory. Here, only four fitting parameters - the upper critical field (B_{c2}), the anisotropy parameter (γ), the pinning force maximum (F_m), and the percolation threshold (P_c) - are needed to describe the field dependence of the critical current for each temperature. We previously reported that for polycrystalline wire samples, the percolation threshold, P_c , is usually 0.26 (Shahabuddin et al. 2014a; Kim et al. 2011).

In Figure 1b, there is a clear upward curvature in the temperature dependence of the upper critical field parallel to the *ab*-plane, B_{c2}^{ab} . The positive curvature is usually related to the two-band nature of MgB₂, for example. All

the lines in Figure 1b are calculated by Equation 2, based on the dirty-limit two-gap theory:

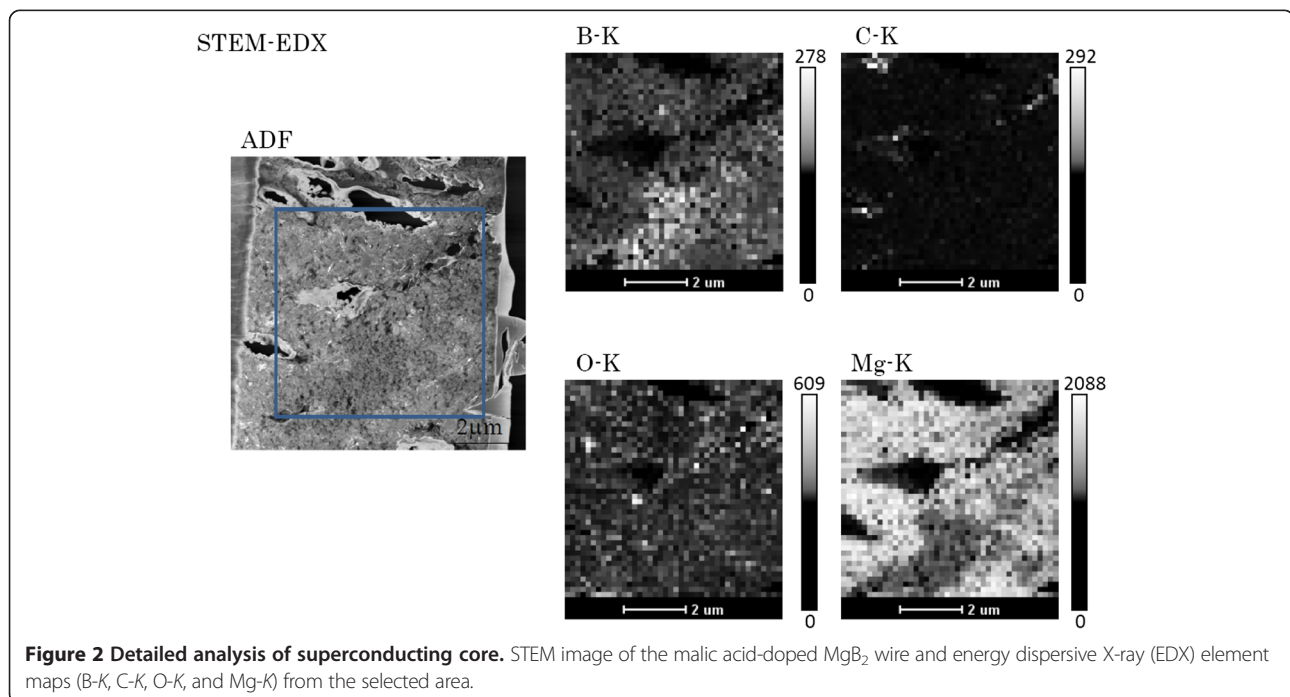
$$2w[\ln t + u(b/t)][\ln t + u(\eta b/t)] + \lambda_2[\ln t + u(\eta b/t)] + \lambda_1[\ln t + u(b/t)] = 0 \quad (2)$$

where t is the reduced temperature T/T_c and b is defined as $\hbar H_{c2} D_\sigma / 2 \phi_0 k_B T_c$, where D_σ is the σ band diffusivity and ϕ_0 is the flux quantum. The function $u(x)$ is defined as $u(x) = \psi(1/2 + x) - \psi(1/2)$, where $\psi(x)$ is the digamma function. η is the ratio of the π band to the σ band diffusivity, D_π/D_σ . w and $\lambda_{1,2}$ can be obtained from the electron-phonon coupling constant λ_{mn} and the Coulomb pseudo-potential matrix μ_{mn} (Gurevich 2003; Shahabuddin et al. 2014b). The electron-phonon coupling constant and the Coulomb pseudo-potential can vary with doping. According to a model calculation based on the two-band Eliashberg theory for MgB_2 (Umharino et al. 2005), the Coulomb pseudo-potential is a slowly decreasing, almost linear function as the carbon content increases. Even within the dirty-limit two-gap theory, interband scattering can affect the transition temperature and the upper critical field (Gurevich 2003). A natural question is then how to work the interband scattering due to carbon doping.

For this purpose, the microstructure observations in a malic acid-doped MgB_2 wire are carried out, as can be seen in Figure 2. We obviously found that there were voids, crystalline MgB_2 , and residual boron precursor. Oxygen (O) is obviously found, indicating the existence of MgO . For example, high concentrated O-K and

magnesium (Mg)-K (indicated by a white color) can be related to the MgO particles (Figure 2). It is noted that MgO particles are inhomogeneously dispersed. To further improve the transport critical current of the MgB_2 superconductor for practical applications, elimination of the voids, MgO , and residual boron powders is very important. Interestingly, the residual boron powders appear even after sintering process. Crystalline MgB_2 grains are found to be blocked by the residual boron powders. It is thus necessary to look into the residual boron precursor.

A high-angle annular dark-field scanning TEM (HAADF-STEM) image of the un-reacted boron phase is shown in Figure 3a. The HAADF-STEM image is obtained with the atomic number dependant contrast (Z-contrast) method, where bright areas correspond to the magnesium (Mg)-rich phase as the atomic number of Mg is higher than any other constituent elements. Within un-reacted boron, lots of nanosized Mg-rich bright spots were observed, and a closer look on these spots reveals that those correspond to crystalline MgB_2 . A high-resolution TEM image and its fast Fourier transform (FFT) pattern, and EELS on both bright spot and the un-reacted boron matrix are shown in Figure 3b,c,d, respectively. These nanosized crystalline MgB_2 (<5 nm) seem to be seeds for further grain growth, and Figure 3a can be regarded as an early stage of MgB_2 crystalline phase growth. From the viewpoint of flux pinning, these MgB_2 nanoparticles with a strong crystalline phase are well distributed. Such fine particles can act as strong flux pinning centers. In addition, the nanosized MgB_2 grains assist in providing excellent wetting and contacting with the coarse MgB_2 grain with highly



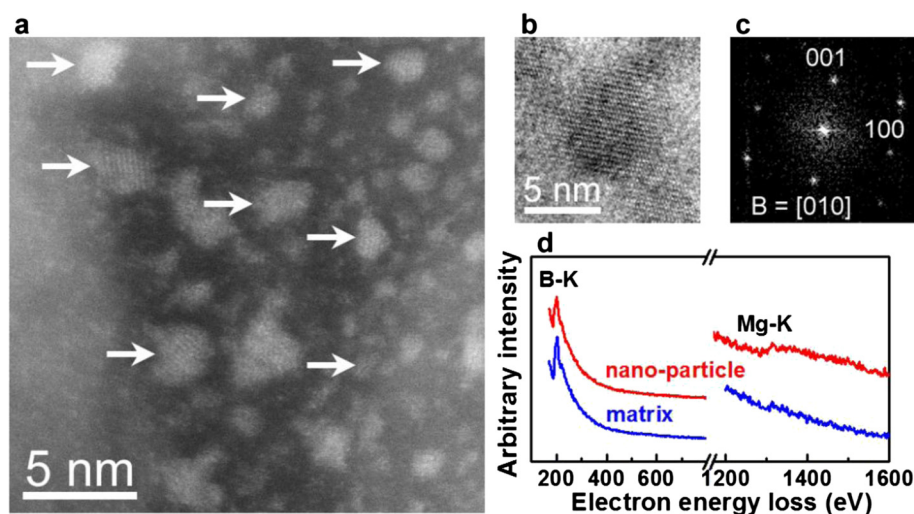


Figure 3 Detailed analysis of un-reacted boron. The region surrounded by residual boron was examined by high-angle annular dark-field scanning TEM. **(a)** Many bright spots corresponding to Mg-rich phase were observed, as indicated by arrows. **(b, c)** Representative high-resolution BF-STEM image of the Mg-rich nanoparticles and its fast Fourier transform. These Mg-rich nanoparticles were found to be the MgB_2 crystalline phase. **(d)** Within the nanoparticles, a small Mg-K EELS peak can be observed.

crystallinity. Thus, these might cause better grain connection as well, as confirmed by the high critical current density under the low-field region. Still, we could not find the carbon element within the MgB_2 grain.

Herein, we also need to further look into a boundary of the MgB_2 grain. We observed the low-angle tilted grain boundary of MgB_2 as shown in Figure 4a through filtered annular dark-field scanning TEM (ADF-STEM). The crystallographic orientation of grain 1 is slightly tilted compared to that of grain 2. The angle between two

grains was estimated to be 5° . The schematic image of the selected grain boundary area is shown in Figure 4b. It is well known that the low-angle tilted grain boundary is the structure of repeated edge dislocations. Edge dislocation was also found in the MgB_2 grain boundary. It is interesting that edge dislocation is formed in the boron (B) plane similar to that within a grain. Some boundary is composed with two magnesium (Mg) planes which are denoted in Figure 4b. The Mg-Mg boundary is formed under the boron extra half plane. In particular, missing B

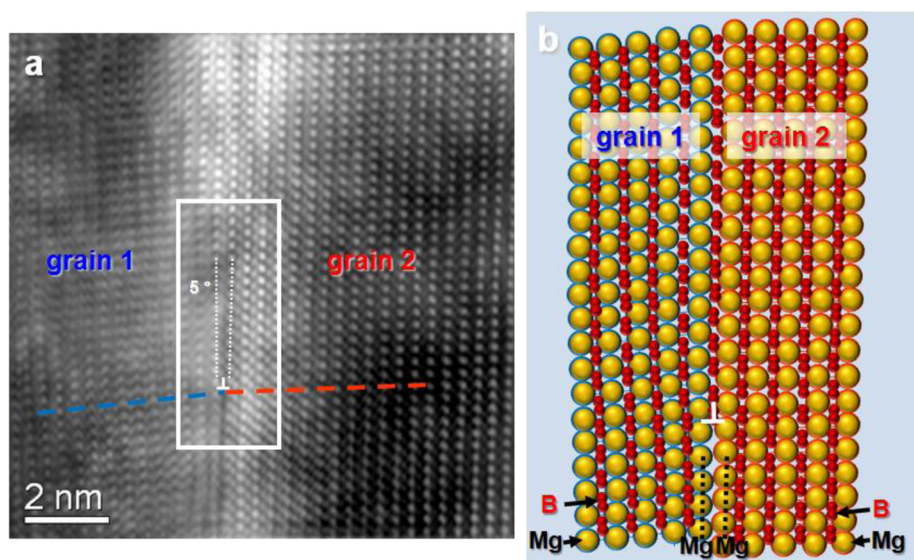


Figure 4 Detailed analysis of the grain boundary. **(a)** Filtered ADF-STEM image of 5° tilted MgB_2 boundary, showing the edge dislocation structure at the boundary. **(b)** Atomistic description of the selected area in **(a)**. The Mg-Mg boundary is observed under only boron extra half plane.

atoms, which were located inside the MgB_2 grain, were observed in our previous work (Kim et al. 2012). Detailed microscopic analysis has shown that B vacancies generate intrinsic stacking faults within the MgB_2 grains, together with associated lattice distortion. Hence, it affects impurity scattering and, thereby, enhances the upper critical field. Therefore, we conclude that carbon ‘doping’ can maximize crystalline imperfection and enhances the superconducting properties.

Conclusions

Our detailed microscopic analyses can be summarized into the following consistent picture on the effect of homogeneous carbon doping during the wire heat treatment process: Magnesium vapor permeates into carbon-shielded boron and forms nanocrystalline MgB_2 seeds. As these seeds grow further, grains merge together, carbon is extruded outside MgB_2 phases, and a small amount of remaining carbon causes lots of defects. Carbon also prevents boron agglomeration, resulting in a dense wire core. Already, the critical current density at low field is comparable to Nb-Ti, and we expect that further optimization can lead the un-reacted boron phase into a fully reacted MgB_2 phase while maintaining its small grain size and a drastic increase in the critical current density far beyond Nb-Ti can be realized.

Competing interests

The authors declare that they have no competing interests.

Authors' contributions

JHK and SC designed the experiments and wrote the manuscript. SC estimated the wire properties, and JHK acquired the TEM experimental data. Both authors read and approved the final manuscript.

Authors' information

JHK is currently an associate professor at the University of Wollongong, Australia. He received his B.S. (1998), M.S. (2000), and Ph.D. (2005) from Sungkyunkwan University, Korea. He has published more than 120 papers in international refereed journals. He is currently acting as an editorial board member for Scientific Reports (Nature Publishing Group). His major research interest is rationally designed materials toward energy storage and harvest applications, including superconducting materials. SC received a B.S. degree in electrical engineering from Sungkyunkwan University, Korea, in 1998. He received his M.S. and Ph.D. degrees in electrical and computer engineering from Sungkyunkwan, Suwon, Korea, in 2000 and 2005, respectively. His thesis for Ph.D. was on discussing an issue on the characteristics and methods of AC losses for superconducting application. From 2006 to 2010, he was a postdoctoral researcher at the Magnet Development Group, Superconducting Materials Center, National Institute for Materials Science, developing a high-field superconducting insert magnet for the 1.05 GHz NMR upgrading project. Since 2010, he has been a senior researcher at the Busan Center, Korea Basic Science Institute. He is currently involved in the development of a superconducting magnet system for a 28 GHz electron cyclotron resonance ion source and heavy ion accelerator. He is also the project leader of the helium-free MgB_2 superconducting magnet development and the superconducting magnet development for physical properties of a superconductor wire.

Acknowledgements

This work was supported by KBSI (Korea Basic Science Institute) Grant T35519 to S. Choi.

Author details

¹Institute for Superconducting and Electronic Materials, University of Wollongong, North Wollongong, New South Wales 2500, Australia. ²Busan Center, Korea Basic Science Institute, Geumjeong, Busan 609-735, Republic of Korea.

Received: 12 January 2015 Accepted: 15 January 2015

Published online: 04 March 2015

References

- Eisterer M (2007) Magnetic properties and critical currents of MgB_2 . *Supercond Sci Technol* 20:R47–R73
- Gurevich A (2003) Enhancement of the upper critical field by nonmagnetic impurities in dirty two-gap superconductors. *Phys Rev B* 67:184515
- Hata S, Sostiati H, Shimada Y, Matsumoto A, Ikeda K, Nakashima H, Kitaguchi H, Kumakura (2013) Imperfection of microstructural control in MgB_2 superconducting tapes fabricated using an in-situ powder-in-tube process: toward practical applications. *J Mater Sci* 48:132
- Jin S, Mavoori H, Bower C, Dover RBV (2011) High critical currents in iron-clad superconducting MgB_2 wires. *Nature* 411:563–565
- Kazakov SM, Puzniak R, Rogacki K, Mironov AV, Zhigadlo ND, Jun J, Soltmann C, Batlogg B, Korus J, Dolgov OV, Kremer RK, Golubov AA (2005) Carbon substitution in MgB_2 single crystals: Structural and superconducting properties. *Phys Rev B* 71:024533
- Kim JH, Dou SX, Shi DQ, Rindfleisch M, Tomsic M (2007) Study of MgO formation and structural defects in in situ processed MgB_2/Fe wires. *Supercond Sci Technol* 20:1026–1031
- Kim JH, Oh S, Kumakura H, Matsumoto A, Heo YU, Song KS, Kang YM, Maeda M, Rindfleisch M, Tomsic M, Choi S, Dou SX (2011) Tailored materials for high-performance MgB_2 wire. *Adv Mater* 23:4942–4946
- Kim JH, Oh S, Heo YU, Hata S, Kumakura H, Matsumoto A, Mitsuhashi M, Choi S, Shima Y, Maeda M, MacManus-Driscoll JL, Dou SX (2012) Microscopic role of carbon on MgB_2 wire for critical current density comparable to NbTi. *NPG Asia Mater* 4:E3
- Korus J, Dolgov OV, Kremer RK, Golubov AA (2005) Carbon substitution in MgB_2 single crystal: structural and superconducting properties. *Phys Rev Lett* 94:027002
- Maeda M, Kim JH, Oh S, Li WX, Takase K, Kuroiwa Y, Dou SX, Takano Y (2013) Enhancing the superconducting properties of magnesium diboride without doping. *J Am Ceram Soc* 96:2893–2897
- Nagamatsu J, Nakagawa N, Muranaka T, Zenitani Y, Akimitsu J (2001) Superconductivity at 39 K in magnesium diboride. *Nature* 410:63–64
- Patel D, Hossain MSA, Motaman A, Barua S, Shahabuddin M, Kim JH (2014) Rational design of MgB_2 conductors toward practical applications. *Cryogenics* 63:160–165
- Shahabuddin M, Alzayed NS, Oh S, Choi S, Maeda M, Hata S, Shimada Y, Hossain MSA, Kim JH (2014a) Microstructural and crystallographic imperfections of MgB_2 superconducting wire and their correlation with the critical current density. *AIP Adv* 4:017113
- Shahabuddin M, Alzayed NS, Oh S, Choi S, Maeda M, Shah MS, Motaman A, Hossain MSA, Kim JH (2014b) Percolative nature of current transport in polycrystalline MgB_2 wires. *Solid State Commun* 181:20–23
- Susner MA, Bohnenstiehl SD, Dregia SA, Sumption MD, Yang Y, Donovan JJ, Collings EW (2014) Homogeneous carbon doping of magnesium diboride by high-temperature, high-pressure synthesis. *Appl Phys Lett* 104:162603
- Ummarino GA, Daghero D, Gonnelli RS, Moudouh AH (2005) Carbon substitutions in MgB_2 within the two-band Eliashberg theory. *Phys Rev B* 71:134511